

Single-atom anchored novel two-dimensional MoSi₂N₄ monolayers for efficient electroreduction of CO₂ to formic acid and methane

Wei Xun^{a*}, Xiao Yang^a, Qing-Song Jiang^a, Ming-Jun Wang^{b*}, Yin-Zhong Wu^c, Ping Li^{d*}

^a Faculty of Electronic Information Engineering, Huaiyin Institute of Technology, Huaian 223003, China (xunwei@hyit.edu.cn)

^a Faculty of Electronic Information Engineering, Huaiyin Institute of Technology, Huaian 223003, China (yangxiao@hyit.edu.cn)

^a Faculty of Electronic Information Engineering, Huaiyin Institute of Technology, Huaian 223003, China (jiangqingsong05@hyit.edu.cn)

^b School of Automation and Information Engineering, Xi'an University of Technology, Xi'an, Shaanxi 710048, China (wangmingjun@xaut.edu.cn)

^c School of Physical Science and Technology, Suzhou University of Science and Technology, Suzhou 215009, China (yzwu@usts.edu.cn)

^d State Key Laboratory for Mechanical Behavior of Materials, Center for Spintronics and Quantum System, School of Materials Science and Engineering, Xi'an Jiaotong University, Xi'an, Shaanxi 710049, China (pli@xjtu.edu.cn)

Abstract

Efficient and selective CO₂ electroreduction into value-added chemicals and fuels emerged as a significant approach for CO₂ conversion, however, it relies on catalysts with controllable product selectivity and reaction paths. In this work, by means of first-principles calculations, we identify five catalysts (TM@MoSi₂N₄, TM = Sc, Ti, Fe, Co and Ni) comprising transition-metal atoms anchored on a MoSi₂N₄ monolayer, whose catalytic performance can be controlled by adjusting the *d*-band center and occupation

of supported metal atoms. During CO₂ reduction, the single metal atoms function as the active sites activates the MoSi₂N₄ inert basal-plane, and as-designed electrocatalysts exhibit excellent activity in CO₂ reduction. Interestingly, HCOOH is the preferred product of CO₂ reduction on the Co@MoSi₂N₄ catalyst with a rate-determining barrier of 0.89 eV, while the other four catalysts prefer to reduce CO₂ to CH₄ with a rate-determining barrier of 0.81-1.24 eV. Moreover, MoSi₂N₄ is an extremely-air-stable material, which will facilitate its application in various environments. Our findings provide a promising candidate with high activity, catalysts for renewable energy technologies, and selectivity for experimental work.

Keywords: Electrochemical CO₂ reduction; Single atom catalysts; 2D materials; Density functional theory

1. INTRODUCTION

Because of the continuing increase in the emissions of CO₂ from excessive fossil fuel usage, the reduction of CO₂ into environmentally friendly, high-efficiency, and low-cost alternative fuels such as formic acid (HCOOH), methanol (CH₃OH), and methane (CH₄) is recognized as one of the most promising approaches that would positively impact the global carbon balance and energy storage¹⁻⁶. Since CO₂ is an extremely stable and nonreactive molecule, converting CO₂ into fuels is a scientifically challenging problem requiring appropriate catalysts and high energy input². Single atom catalysts (SACs), first proposed for CO oxidation in 2011⁷, provide efficient activation and conversion of CO₂ using transition metal (TM) atoms⁸⁻¹⁶. The coexistence of empty and occupied TM *d*-orbitals can accept lone-pair electrons, and then back-donate these electrons to the antibonding orbitals to weaken the C=O bonds.

Remarkably, since two dimensional (2D) materials have large surface-to-volume ratios, short carrier diffusion distances, unique electronic properties, and abundant active sites, they serve as promising substrates for atomically dispersed transition metal atoms for CO₂ reduction. To date, most of the discovered monolayer 2D materials have

a thickness of $n \leq 7$. Graphene monolayer is famous six-membered ring (SMR) materials¹⁷ of $n = 1$, which have been a central topic for CO₂ reduction^{18–28}. The silicon counterpart of graphene ($n = 2$), has also shown great potential for CO₂ reduction^{29,30}. For $n = 3$, monolayer transition-metal dichalcogenides are the most studied SMR materials. In particular, the reduction of CO₂ to methanol can be achieved with the MoS₂ supported single Co atom catalyst³¹. Among the family of $n = 4$, monolayer group III chalcogenides have attracted growing interest. For instance, TM@InSe catalysts based on 2D InSe and transition metal atoms are candidates for CO, HCOOH, and CH₄ production³². The 2D In₂Se₃, the representative systems of $n = 5$, Anchoring different single TM atoms shows the great electrocatalytic ability of CO₂ reduction via ferroelectric switching³³. Recently, CaMg was found to have a sextuple layer ($n = 6$) structure, but there is no research about CO₂ reduction³⁴.

Recently, a new compound of septuple layer SMR material, MoSi₂N₄, has been successfully, which has a band-gap of ~ 1.94 eV with excellent ambient stability³⁵. The MoSi₂N₄ monolayer can be built by intercalating a 2H-MoS₂-type MoN₂ layer ($n = 3$) into an α -InSe-type Si₂N₂ ($n = 4$). Motivated by the extensive research attention of MoSi₂N₄ and the reported interesting electronic and catalytic properties^{36–46}, it is of great fundamental interest to determine whether the emerging 2D MoSi₂N₄ materials can be applied to other important electrocatalytic reactions, such as the CO₂ reduction reaction (CO₂RR).

In this work, we theoretically investigate the potential of using transition metal decorated MoSi₂N₄ monolayers for electrochemical CO₂ reduction into hydrocarbon fuels. Our efforts identify five catalysts with singly dispersed TM atoms anchored on the 2D MoSi₂N₄ monolayer (denoted as TM@MoSi₂N₄, where TM = Sc, Ti, Fe, Co and Ni). The differential charge density demonstrated that TM atoms form strong interactions with MoSi₂N₄ by exchanging electron density. With the increase in atomic number, the net electron transfer of TM atoms to CO₂ decreases, indicating that CO₂ activation changes from strong to weak. Anchoring different TM atoms can not only alter the reaction barrier and paths of CO₂ reduction, but also lead to different final products. These performance improvements stem from the synergistic effects of the

adjusted empty and occupied *d*-orbitals (*d* orbital center) of the adsorbed metal atom, electron transfer, and CO₂ adsorption energies. These SACs and catalytic mechanisms introduce a feasible approach to significantly improve the efficiency of the CO₂RR.

2. COMPUTATIONAL METHODS

DFT calculations were performed by using the Vienna Ab Initio Simulation Package (VASP)^{47, 48}. The exchange–correlation interactions were treated within the generalized gradient approximation (GGA)⁴⁹ in the form of the Perdew–Burke–Ernzerhof (PBE) functional⁵⁰. The van der Waals interactions were described using the Bayesian Error Estimation Exchange–correlation functional (BEEF-vdw)⁵¹. The electron wave functions were expanded using plane waves with a cutoff energy of 500 eV, and the convergence criteria for the residual force and energy on each atom during structure relaxation were set to 0.002 eV/Å and 10^{−6} eV, respectively. The vacuum space was more than 20 Å, which was enough to avoid interactions between periodic images. The dipole correction is taken into account for all the asymmetric structures⁵². The single-atom catalysts were modelled by depositing one metal atom on 2×2×1 supercell MoSi₂N₄. The Brillouin zone (BZ) was sampled with a Monkhorst–Pack mesh with a 6 × 6 × 1 kpoint grid in reciprocal space during geometry optimization, and a 12×12×1 kpoint grid to calculate the electronic properties of all systems. The Gibbs free energy is calculated using a hydrogen electrode model (CHE)⁵³, and the solvent effect is considered with the implicit solvent model implemented in VASPsol^{33, 54}. The site-specific charge differences were obtained using Bader analysis.

3. RESULTS AND DISCUSSION

Due to the large band gap (1.94 eV) of the MoSi₂N₄ monolayer, not enough electrons are injected into the antibonding 2π_u orbitals of CO₂ so that the strong *sp*-hybridization symmetry of the carbon atom cannot be disrupted⁵⁵. Therefore, the MoSi₂N₄ material itself is not suitable as a catalyst for CO₂ reduction. Our theoretical study also confirmed this point: by adsorption on MoSi₂N₄, the inherent linear O=C=O structure of CO₂ molecules can be well maintained (see Supplementary Fig. S1).

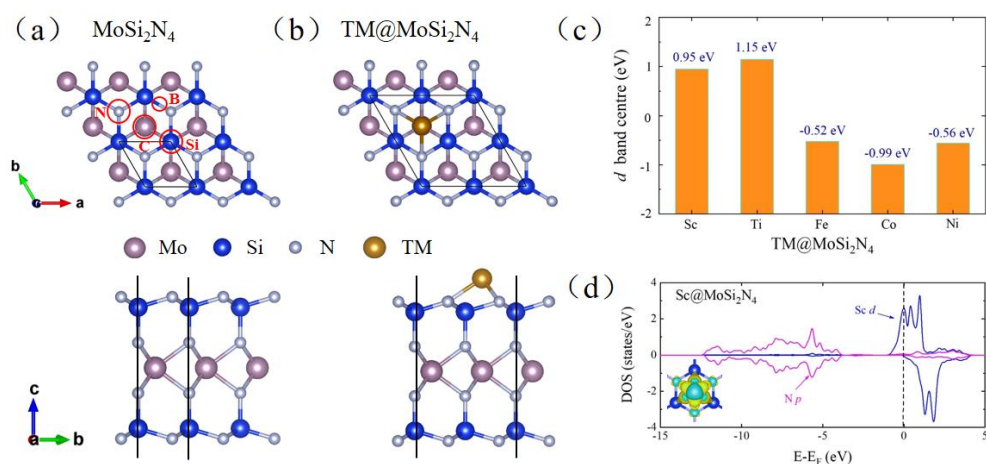


Fig. 1 Geometries and electronic structures of the MoSi₂N₄ catalysts. Top and side views of the optimized MoSi₂N₄ monolayer without transition metal atoms (a) and with transition metal atoms (b). Red circles denote selected adsorption sites: N, top of the N atom; B, top of the Si-N bond; Si, top of the Si atom; C, center of the six-membered ring. The black rhombus represents the unitcell of MoSi₂N₄ and supercell of TM@MoSi₂N₄. (c) The *d* band center of TM@MoSi₂N₄ (TM = Sc, Ti, Fe, Co and Ni). (d) The partial density of states of Sc@MoSi₂N₄. The isosurfaces are 0.005 e/Å³.

To activate CO₂ electrochemical reduction, we introduce transition metal atoms to modify the MoSi₂N₄ monolayer and provide additional electrons to break strong *sp* hybridization, to activate CO₂ molecules. Compared with traditional metal catalysts, SACs usually show higher catalytic performance because of their high low-coordination configuration ratio. However, transition metals must be screened because only SACs with well empty/occupied *d* orbitals balanced can show the best catalytic performance^{7, 33, 56, 57}. To find suitable SACs, 10 transition metal atoms (*3d*) were selected for chemisorption on the monolayer surface of MoSi₂N₄ and the most favorable energy configuration was determined (see Supplementary Fig. S2). Then, we evaluated all composites against two key criteria. Firstly, in order to ensure the stability of the active center, a single transition metal atom should be stably adsorbed on the surface of MoSi₂N₄ monolayer without destroying the underlying structure. Second, a single transition metal atom should be able to activate CO₂, that is, the linear structure of O=C=O should decompose after adsorption. After comprehensively studying the

adsorption configuration with the most favorable energy (Fig. 1a, 1b) and its stability, we selected five TM atoms (TM=Sc, Ti, Fe, Co and Ni) as promising CO₂ reduction catalysts for further study. The other five candidates are either unstable (TM=Mn, Zn) or not effective at activating CO₂ molecules (TM=V, Cr, Cu) (see Supplementary Fig. S3). To further demonstrate the structural stability of the SACs chosen in this study, ab initio molecular dynamics (AIMD) simulations were also performed at TM@MoSi₂N₄ with a Nose-Hoover thermostat at 300 K. In the AIMD simulations, the metal atoms were anchored in energetically favorable positions for at least 15 ps, even at room temperature (300 K) (see Supplementary Figure S4).

Table 1 Parameters for the pure TM@MoSi₂N₄ and CO₂ adsorbed TM@MoSi₂N₄: adsorption site (S_{ad}), binding energies of TM atom (E_{b-TM} in eV/atom) and CO₂ molecule (E_{b-CO_2} in eV/molecule), charge lost from the adsorbed TM atoms (Q_{TM} in e/atom), average TM-N bond length (l_{TM-N} in Å), charge gained by the adsorbed CO₂ molecule (Q_{CO_2} in e/molecule), and bond angle ($\angle OCO$ in °).

Catalysts	S_{ad}	E_{b-TM}	Q_{TM}	l_{TM-N}	E_{b-CO_2}	Q_{CO_2}	$\angle OCO$
Sc@MoSi ₂ N ₄	C	-0.60	1.45	2.51	-2.72	1.10	127.3
Ti@MoSi ₂ N ₄	C	-0.81	1.38	2.43	-2.11	1.05	129.5
Fe@MoSi ₂ N ₄	C	-0.12	0.74	2.08	-1.26	0.65	142.5
Co@MoSi ₂ N ₄	C	-0.41	0.50	2.07	-1.46	0.42	147.8
Ni@MoSi ₂ N ₄	C	-1.17	0.46	2.06	-1.52	0.45	147.4

At the most energetically favorable positions, all five TM atoms have strong binding energies (Table 1), indicating that the interaction between the metal atom and the base is strong enough, as seen from the strong TM-N bond (Fig. 1a and supplementary Fig. S5). Chemical bond interactions can be illustrated by the large accumulation of partial charges between TM atoms and surrounding N atoms (see Table 1 and supplementary Fig. S5) and the strong hybridization of N *p* and TM *d* orbitals

(see Fig. 1d and supplementary Fig. S6). The average TM-N bond length, binding energy and electron transfer are shown in Table 1. As the atomic number of metals increases, TM@MoSi₂N₄ usually has a shorter average TM-N bond length and less electron transfer. The balance between the empty and occupied *d* orbitals caused by electron transfer has a significant impact on the TM@MoSi₂N₄ catalytic activity. With Sc@MoSi₂N₄ as an example, the charge is redistributed between the Sc atom and N atom (see Fig. 1d), and the *d* orbital of the Sc atom is exhausted. Compared with Ni@MoSi₂N₄ (0.46 e, see supplementary Fig. S6), Sc@MoSi₂N₄ has more electron transfer (1.45 e), and the Sc-*d* orbital moves to higher energies. As shown in Fig. 1c, the *d*-band center of Sc@MoSi₂N₄ (0.95 eV) is higher than that of Ni@MoSi₂N₄ (-0.56 eV), indicating that Sc@MoSi₂N₄ has a better catalytic capacity⁵³. Under the same mechanism, the other four TM@MoSi₂N₄ catalysts show a similar phenomenon (see Fig. 1c): the *d*-band center of the TM atom moves in a lower energy direction as the metal atomic number increases. Note that TM@MoSi₂N₄ (TM = Sc, Ti) and TM@MoSi₂N₄ (TM = Fe, Co, Ni) have little difference in their *d*-band center positions. These comparisons show that both reaction paths and barriers are influenced by metal atoms (see detailed classification of catalysis below).

The effective activation of CO₂ molecules is the key to subsequent reduction. According to the structural analysis, all TM@MoSi₂N₄ catalysts can effectively activate CO₂ molecules by forming bidentate C-TM-O species (see Fig. 2 and supplementary Fig. S7). In addition, the binding energy of catalysts with active CO₂ molecules (-2.72 to -1.26 eV; see Table 1) is equivalent to the reported catalysts^{28, 33, 50}. Strong hybridization of O-*p* orbitals and TM-*d* orbitals and significant charge transfer between TM@MoSi₂N₄ and CO₂ ensure that inert molecules are chemically captured (see Fig. 2a, 2b and Supplementary Fig. S7). Note that the activation degree of CO₂ can be clearly seen from the angles of ∠OCO (see Table 1). At the same time, the activation degree of CO₂ on TM@MoSi₂N₄ (TM = SC, Ti) was significantly higher than that on TM@MoSi₂N₄ (TM = Fe, Co, Ni), as shown by the greater binding energy (- 2.72 ~ - 2.11 eV vs -1.26 ~ -1.52 eV), more electron transfer (1.05 ~ 1.1 e vs 0.42 ~ 0.65 e) and smaller ∠OCO angle (127.3° ~ 129.5° vs 142.5° ~ 147.8°).

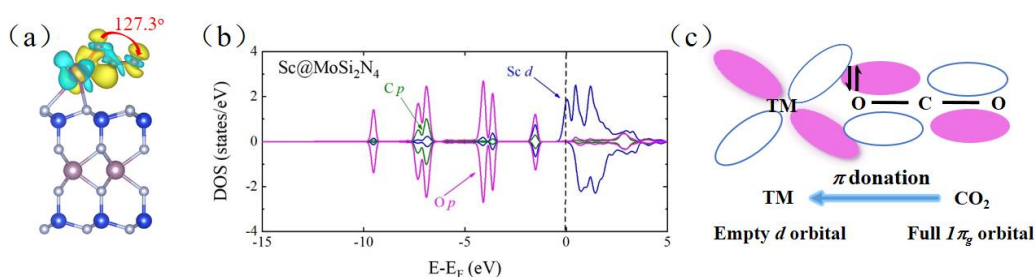


Fig. 2 Transition metal atom activated CO₂. (a) The differential charge density plots and (b) partial density of states of CO₂ adsorbed on Sc@MoSi₂N₄. (c) Simplified schematic diagrams of CO₂ bonding to transition metal atoms.

The diverse behavior of CO₂ on different surfaces is attributed to the catalytic activation mechanism of CO₂, i.e., the coexistence of charge dissipation and accumulation between TM atoms and CO₂ molecules. The empty TM *d* orbital can accept electrons from the highest occupied molecular orbital ($1\pi_g$ orbital) in the CO₂ molecule (Fig. 2c). The synergistic effect of electron reception, feedback, and *d*-orbital occupation ensures that CO₂ can be activated efficiently. The isolated Sc atom has only one electron occupying the *d* orbital ($3d^1$). After adsorption on the MoSi₂N₄ substrate, the Sc atom loses part of its *d* electrons, forming a Sc-N bond, and the resulting empty Sc *d* orbital provides a channel for electron acceptance and donation to activate the CO₂ molecule. Compared with other TM@MoSi₂N₄ catalysts, under the circumstance that the intrinsic part of the TM atom occupies the *d* orbital, the Sc@MoSi₂N₄ catalyst has a higher degree of CO₂ activation, a relatively smaller angle $\angle\text{OCO}$ and a larger charge transfer (see Table 1).

As an important competitive side reaction, hydrogen evolution (HER) may significantly inhibit the Faraday efficiency of the CO₂RR by depleting the proton-electron pairs in electrolyte solutions^{58, 59}. To verify whether the CO₂RR is more favorable, we first calculated the change in Gibbs free energy (ΔG) in the first step of CO₂RR ($*+\text{CO}_2+\text{H}^++\text{e}^- \rightarrow \text{OCOH}^*$ or OCHO^*) and HER ($*+\text{H}^++\text{e}^- \rightarrow \text{H}^*$). According to Brønsted Evans Polanyi relations^{60, 61}, reactions with lower ΔG values have smaller reaction barriers and are therefore more dynamically advantageous.

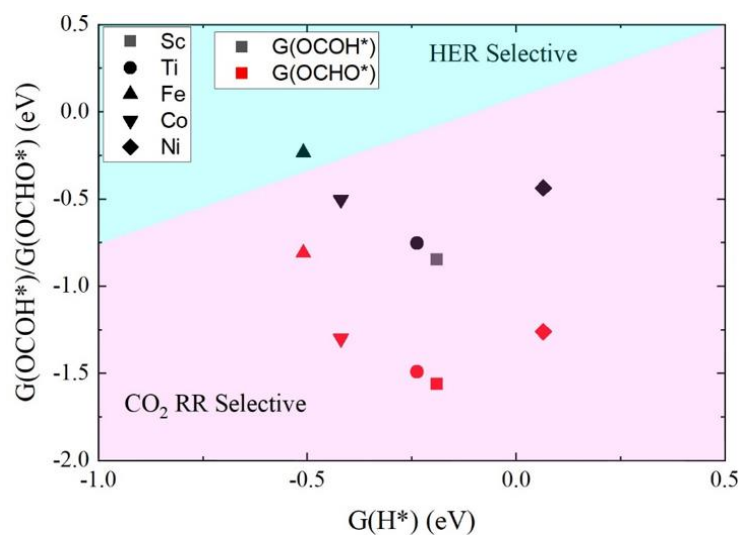


Fig. 3 Selectivity for CO₂RR vs HER. Gibbs free energy changes (ΔG) of the initial protonation of CO₂RR vs. HER on TM@MoSi₂N₄ (TM= Sc, Ti, Fe, Co and Ni). Data points in the purple region indicate higher selectivity toward the CO₂RR, while those in the blue region indicate higher selectivity toward the HER. Black and red symbols represent ΔG (OCOH*) vs ΔG (H*) and ΔG (OCHO*) vs ΔG (H*), respectively.

To a clearer understanding of the mechanism, we investigate the possible reaction pathways of the CO₂RR on TM@MoSi₂N₄, as shown in Figure 4. During CO₂RR, the reaction includes eight elemental hydrogenation steps, which are determined by the most stable product at each step. The initial step of CO₂RR is the formation of OCHO*,

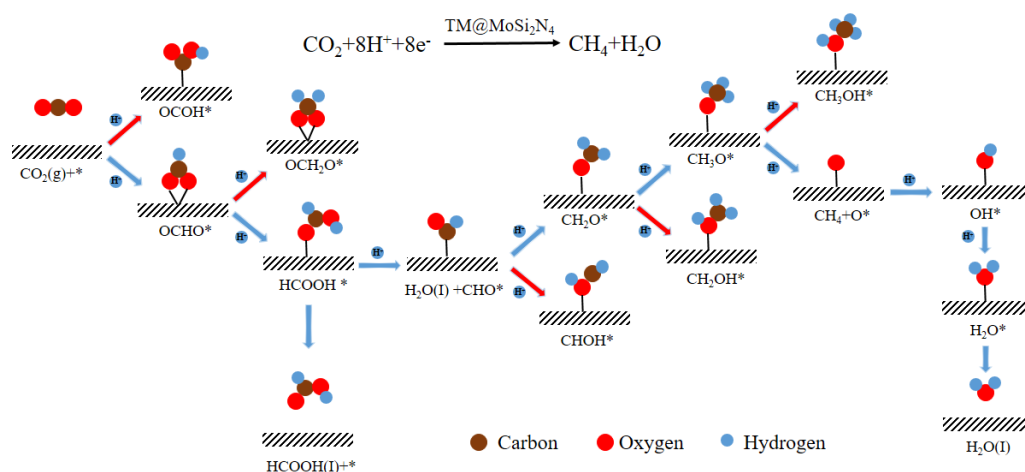
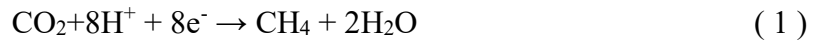


Fig. 4 Possible reaction pathways of the CO₂RR on TM@MoSi₂N₄, where * indicates the adsorption site on the MoSi₂N₄ surface.

which is followed by the hydrogenation of OCHO* to give HCOOH*. (OCHO* + H⁺ + e⁻ → HCOOH*). Note that while the decomposition of HCOOH into CHO* + H₂O (I) is induced by the action of the third hydrogen, desorbed HCOOH (I) + * may also be formed. Here, we need to compare the limiting potentials of the HCOOH (I) + * pathway and subsequent pathways to determine the possible reaction pathways of the CO₂RR. Except for Co@MoSi₂N₄, the other four catalysts follow the HCOOH* + H⁺ + e⁻ → H₂O (I) + CHO* pathway, forming nonabsorbent CH₄ after progressive hydrogenation. The adsorbed O* then hydrogenates to OH*, H₂O*, and desorbed H₂O. All intermediates and products are adsorbed on TM atoms.

The CO₂RR pathways to HCOOH and CH₄ on the TM@MoSi₂N₄ catalyst were studied in detail, as shown in Fig. 5. The overall reaction of CO₂RR to form CH₄ on the Sc@MoSi₂N₄ catalyst in the presence of hydrogen is expressed as follows:



In general, the stronger the adsorption of the intermediates on the catalyst is⁸, the lower the barrier for a chemical reaction that can be obtained. In Fig. 5a, we present the minimum energy pathways for CO₂RR to CH₄ on the Sc@MoSi₂N₄ catalyst.

The pathways for the formation of CH₄ on the Ti@MoSi₂N₄, Co@MoSi₂N₄ and Ni@MoSi₂N₄ catalysts are found to be nearly the same as those on the Sc@MoSi₂N₄ catalyst, but are thermodynamically more favorable because of the stronger interactions between Sc and the reaction intermediates. The barrier for hydrogenation of CHO* to CH₂O* (0.81 eV) during the formation of CH₄ is comparable to that for the hydrogenation of CH₂O* (0.74 eV). It should be noted that such a barrier is much lower than desorbed HCOOH (I) (1.83 eV). Then, CH₂O* is further hydrogenated to CH₃O* and CH₄* with barriers of 0.74 eV. Since the CH₄ product is more thermodynamically stable than HCOOH (I), the formation of CH₄ is likely to be the most dominant reaction pathway on the Sc@MoSi₂N₄ catalyst. For Sc@MoSi₂N₄, the rate-determining step for the formation of CH₄ is the hydrogenation of CHO*, with a barrier of 0.81 eV, which is the same as that for the formation of CH₃O* on the Ti@MoSi₂N₄ catalyst (0.83 eV, see Supplementary Fig. S8). We also investigated the pathway for the reduction of CO₂ on the Fe@MoSi₂N₄ and Ni@MoSi₂N₄ catalysts (see Supplementary Fig. S9, S10). We

found that the interactions between Fe@MoSi₂N₄ (Ni@MoSi₂N₄) and the reactant/intermediates are slightly weak. The weak interactions between the catalyst and the reaction intermediates will lead to a large barrier for the formation of CH₄ on the TM@MoSi₂N₄ catalyst. For instance, the rate-determining step for the Co@MoSi₂N₄ (Ni@MoSi₂N₄) catalysts is the hydrogenation of HCOOH* (the hydrogenation of CH₂O*), with a barrier of 1.18 eV (1.24 eV).

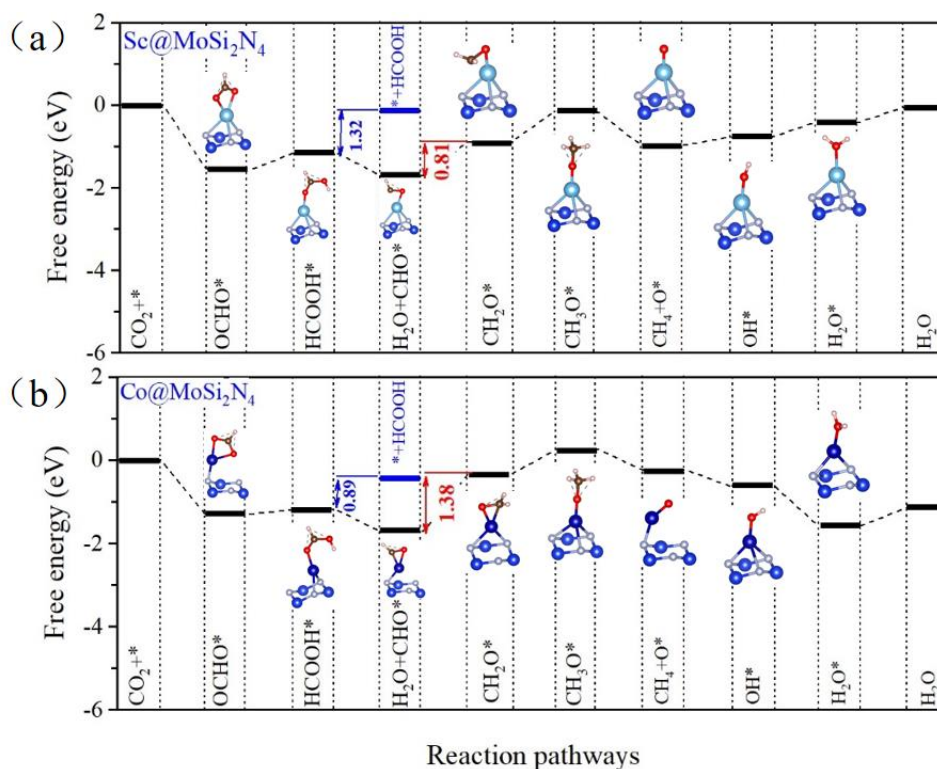


Fig. 5 CO₂RR paths on Sc@MoSi₂N₄ and Co@MoSi₂N₄. Free energy profile for CO₂ electrochemical reduction reactions along the minimum energy path at 0 V (vs. RHE) on (a) Sc@MoSi₂N₄ and (b) Co@MoSi₂N₄. The insets show the optimized configurations of the intermediates.

The formation of HCOOH follows the first two steps of the CH₄ pathway,



Then, HCOOH* desorbs directly from the Co@MoSi₂N₄ catalyst. The rate-determining step of the HCOOH pathway is the second step, with a barrier of 0.89 eV, which is 0.49 eV lower than the rate-determining barrier for the formation of CH₄ (1.38

eV). In addition, the desorption energies of HCOOH on Sc@MoSi₂N₄, Ti@MoSi₂N₄, Fe@MoSi₂N₄ and Ni@MoSi₂N₄, are 1.32 eV, 1.69 eV, 1.89 eV and 1.94 eV, respectively. Therefore, the preferred product for CO₂RR on the Co@MoSi₂N₄ catalyst is the HCOOH pathway rather than the CH₄ pathway

4. CONCLUSIONS

In conclusion, single metal atoms, including Sc, Ti, Fe, Co and Ni, supported on MoSi₂N₄ as electrocatalysts for CO₂RR were investigated by DFT calculations. A single-atom catalyst can not only maximize the efficiency of metal atoms but also exhibit excellent activity for CO₂RR. As evaluated by the reaction barriers, the preferred product of CO₂RR on the Co@MoSi₂N₄ catalyst is HCOOH with a barrier of 0.89 eV, while the Sc@MoSi₂N₄ (Ti@MoSi₂N₄, Fe@MoSi₂N₄ and Ni@MoSi₂N₄) catalyst is able to reduce CO₂ to CH₄ efficiently with a barrier of 0.81 eV (0.83 eV, 1.18 eV and 1.24 eV). These SACs based on 2D materials with thicknesses of $n \geq 7$ hold great promise for improving catalytic activity and selectivity for electrochemical the CO₂RR. Our study not only enriches the understanding of single atom catalysts but also provides clues for further catalyst design for CO₂ electroreduction in theory and experiments.

Acknowledgements

This work is supported by the National Natural Science Foundation of China (Grants No. 12004295). P. Li thanks China's Postdoctoral Science Foundation funded project (Grant No. 2020M673364). This work was calculated at Supercomputer Center in Suzhou University of Science and Technology.

References

1. Olah, G. A., Prakash, G. K. & Goepfert, A. Anthropogenic chemical carbon cycle for a sustainable future. *J. Am. Chem. Soc.* 133, 12881-12898 (2011).
2. Benson, E. E. Kubiak, C. P. Sathrum, A. J. Smieja, J. M. Electrocatalytic and homogeneous approaches to conversion of CO₂ to liquid fuels. *Chem. Soc. Rev.* 38, 89-99 (2009)
3. Li, C. W. Ciston, J. Kanan, M. W. Electroreduction of carbon monoxide to liquid fuel on oxide-derived nanocrystalline copper. *Nature* 508, 504-507 (2014)

- Li, F.-F.; Lau, J.; Licht, S. Sungas Instead of Syngas: Efficient Coproduction of CO and H₂ with a Single Beam of Sunlight. *Adv. Sci.* 2, 1500260 (2015)
- Savéant, J.-M. Molecular catalysis of electrochemical reactions. Mechanistic aspects. *Chem. Rev.* 108, 2348-2378 (2008).
- Qiao, J., Liu, Y., Hong, F. & Zhang, J. A review of catalysts for the electroreduction of carbon dioxide to produce low-carbon fuels. *Chem. Soc. Rev.* 43, 631-675 (2014).
- Qiao, B. et al. Single-atom catalysis of CO oxidation using Pt₁/FeO_x. *Nat. Chem.* 3, 634-641 (2011).
- Gao, G., Jiao, Y., Waclawik, E. R. & Du, A. Single atom (Pd/Pt) supported on graphitic carbon nitride as an efficient photocatalyst for visible-light reduction of carbon dioxide. *J. Am. Chem. Soc.* 138, 6292-6297 (2016).
- Ling, C., Li, Q., Du, A. & Wang, J. Computation-aided design of single-atom catalysts for one-pot CO₂ capture, activation, and conversion. *ACS Appl. Mater. Interfaces* 10, 36866-36872 (2018).
- Zhao, C. et al. Solid-diffusion synthesis of single-atom catalysts directly from bulk metal for efficient CO₂ reduction. *Joule* 3, 584-594 (2019).
- Liu, S. et al. Elucidating the electrocatalytic CO₂ reduction reaction over a model single-atom Nickel catalyst. *Angew. Chem. Int. Ed.* 59, 798-803 (2020).
- Liu, J. et al. Rare Earth single-atom catalysts for nitrogen and carbon dioxide reduction. *ACS Nano* 14, 1093-1101 (2020).
- Samantaray, M. K. et al. The comparison between single atom catalysis and surface organometallic catalysis. *Chem. Rev.* 120, 734-813 (2020).
- Cai YM., et al, Insights on forming N,O-coordinated Cu single-atom catalysts for electrochemical reduction CO₂ to methane, *Nat. Commun.*, 12, 586 (2021).
- Guo YB., Yao S, Xue YY., Hu X, Cui HJ., Zhou Z, Nickel single-atom catalysts intrinsically promoted by fast pyrolysis for selective electroreduction of CO₂ into CO. *Appl. Catal. B Environ.* 304, 120997 (2022).
- Hung, SF., Xu, A., Wang, X. et al. A metal-supported single-atom catalytic site enables carbon dioxide hydrogenation. *Nat. Commun.*, 13, 819 (2022).
- Liu, G., Chen, X.-Q., Liu, B., Ren, W. & Cheng, H.-M. Six-membered-ring inorganic

- materials: definition and prospects. *Natl Sci. Rev.* 8, 248 (2021).
18. Hu HW., et al, Graphene-assisted construction of electrocatalysts for carbon dioxide reduction. *Chem. Eng. J.* 425, 130587 (2021).
 19. K. Jiang, S. Siahrostami, T. Zheng, Y. Hu, S. Hwang, E. Stavitski, Y. Peng, J. Dynes, M. Gangisetty, D. Su, K. Attenkofer, H. Wang, Isolated Ni single atoms in graphene nanosheets for high-performance CO₂ reduction, *Energ. Environ. Sci.* 11, 893-903 (2018).
 20. P. Huang, M. Cheng, H. Zhang, M. Zuo, C. Xiao, Y.i. Xie, Single Mo atom realized enhanced CO₂ electro-reduction into formate on N-doped graphene, *Nano Energy* 61, 428-434 (2019).
 21. P. Su, K. Iwase, S. Nakanishi, K. Hashimoto, K. Kamiya, Nickel-Nitrogen-Modified Graphene: An Efficient Electrocatalyst for the Reduction of Carbon Dioxide to Carbon Monoxide, *Small* 12, 6083-6089 (2016).
 22. A.S. Varela, M. Kroschel, N.D. Leonard, W. Ju, J. Steinberg, A. Bagger, J. Rossmeisl, P. Strasser, pH Effects on the Selectivity of the Electrocatalytic CO₂ Reduction on Graphene-Embedded Fe-N-C Motifs: Bridging Concepts between Molecular Homogeneous and Solid-State Heterogeneous Catalysis, *ACS Energy Lett.* 3, 812-817 (2018).
 23. Z. Chen, K. Mou, S. Yao, L. Liu, Zinc-Coordinated Nitrogen-Codoped Graphene as an Efficient Catalyst for Selective Electrochemical Reduction of CO₂ to CO, *ChemSusChem* 11, 2944-2952 (2018).
 24. C. Jia, K. Ching, P.V. Kumar, C. Zhao, N. Kumar, X. Chen, B. Das, Vitamin B-12 on Graphene for Highly Efficient CO₂ Electroreduction, *ACS Appl. Mater. Interfaces* 12, 41288-41293 (2020).
 25. X. Li, G. Chai, X. Xu, J. Liu, Z. Zhong, A. Cao, Z. Tao, W. You, L. Kang, Electrocatalytic reduction of CO₂ to CO over iron phthalocyanine-modified graphene nanocomposites, *Carbon* 167, 658-667 (2020).
 26. X. Zhang, W. Wang, Z. Yang, CO₂ Reduction on Metal- and Nitrogen-Codoped Graphene: Balancing Activity and Selectivity via Coordination Engineering, *ACS Sustainable Chem. Eng.* 8, 6134-6141 (2020).
 27. Z. Wang, J. Zhao, Q. Cai, CO₂ electroreduction performance of a single transition metal atom supported on porphyrin-like graphene: a computational study, *Phys. Chem. Chem.*

- Phys. 19, 23113-23121 (2017).
28. X. Cui, W. An, X. Liu, H. Wang, Y. Men, J. Wang, C₂N-graphene supported single atom catalysts for CO₂ electrochemical reduction reaction: mechanistic insight and catalyst screening, *Nanoscale* 10, 15262-15272 (2018).
 29. Si Zhou, Wei Pei, Jijun Zhao and Aijun Du, Silicene catalysts for CO₂ hydrogenation: the number of layers controls selectivity. *Nanoscale*, 11, 7734 (2019).
 30. Chenxi Qian et al. Catalytic CO₂ reduction by palladium-decorated silicon-hydride nanosheets. *Nat. Catal.* 2, 46-54 (2019).
 31. Zhansheng Lu, Yingjie Cheng, Shuo Lic, Zongxian Yanga, Ruqian Wu, CO₂ thermoreduction to methanol on the MoS₂ supported single Co atom catalyst: A DFT study. *Appl. Surf. Sci.* 528, 147047 (2020).
 32. Chen-Xu Zhao, Guo-Xu Zhang, Wang Gao and Qing Jiang, Single metal atoms regulated flexibly by a 2D InSe substrate for CO₂ reduction electrocatalysts. *J. Mater. Chem. A*, 7, 8210 (2019).
 33. Lin Ju, Xin Tan, Xin Mao, Yuantong Gu, Sean Smith, Aijun Du, Zhongfang Chen , Changfeng Chen & Liangzhi Kou, Controllable CO₂ electrocatalytic reduction via ferroelectric switching on single atom anchored In₂Se₃ monolayer. *Nat. Commun.* 12, 5128 (2021).
 34. Zhou, J. et al. 2DMatPedia, an open computational database of two dimensional materials from top-down and bottom-up approaches. *Sci. Data* 6, 1-10 (2019).
 35. Hong, Y.-L., et al. Chemical vapor deposition of layered two-dimensional MoSi₂N₄ materials. *Science* 369, 670-674 (2020).
 36. Mortazavi, B. Javvaji, B. Shojaei, F. Rabczuk, T. Shapeev, A. V. Zhuang, X. Exceptional Piezoelectricity, High Thermal Conductivity and Stiffness and Promising Photocatalysis in Two-Dimensional MoSi₂N₄ Family Confirmed by First-Principles. *Nano Energy* 82, 105716 (2021).
 37. B. Li, J. Geng, H. Ai, Y. Kong, H. Bai, K. H. Lo, K. W. Ng, Y. Kawazoe, H. Pan, Design of 2D Materials-MSi₂C_xN_{4-x} (M = Cr, Mo, and W; X = 1 and 2)-with Tunable Electronic and Magnetic Properties. *Nanoscale* 13, 8038-8048 (2021).
 38. S. Li, W. Wu, X. Feng, S. Guan, W. Feng, Y. Yao, S. A. Yang, Valley-Dependent Properties

- of Monolayer MoSi₂N₄, WSi₂N₄, and MoSi₂As₄. *Phys. Rev. B: Condens. Matter Mater. Phys.* 102, 113102 (2020).
39. C. Yang, Z. Song, X. Sun, J. Lu, Valley Pseudospin in Monolayer MoSi₂N₄ and MoSi₂As₄. *Phys. Rev. B: Condens. Matter Mater. Phys.* 103, 035308 (2021).
 40. J. Chen, Q. Tang, The Versatile Electronic, Magnetic and Photo-Electro Catalytic Activity of a New 2D MA₂Z₄ Family. *Chem. Eur. J.* 27, 9925-9933 (2021).
 41. Yuping Chen, Shufang Tian, and Qing Tang, First-Principles Studies on Electrocatalytic Activity of Novel Two-Dimensional MA₂Z₄ Monolayers toward Oxygen Reduction Reaction. *J. Phys. Chem. C* 125, 22581-22590 (2021).
 42. Yadong Yu, Jian Zhou, Zhonglu Guo and Zhimei Sun, Novel Two-Dimensional Janus MoSiGeN₄ and WSiGeN₄ as Highly Efficient Photocatalysts for Spontaneous Overall Water Splitting. *ACS Appl. Mater. Interfaces* 13, 28090-28097 (2021).
 43. Asha Yadav, Jiban Kangsabanik, Nirpendra Singh, and Aftab Alam, Novel Two-Dimensional MA₂N₄ Materials for Photovoltaic and Spintronic Applications. *J. Phys. Chem. Lett.* 12, 10120-101127 (2021).
 44. Nsajigwa Mwankemwa, Hong-En Wang, Ting Zhu, Qiang Fan, Fuchun Zhang, Weibin Zhang, First principles calculations investigation of optoelectronic properties and photocatalytic CO₂ reduction of (MoSi₂N₄)_{5-n}/(MoSiGeN₄)_n in-plane heterostructures. *Results Phys.* 37, 105549 (2022).
 45. Jing Xu, Qingfeng Wu, Zhiyuan Sun, Nsajigwa Mwankemwa, Weibin Zhang, Wenxing Yang, First-principles investigations of electronic, optical, and photocatalytic properties of Au-adsorbed MoSi₂N₄ monolayer. *J. Phys. Chem. Solids* 162, 110494 (2022).
 46. Chengwei Xiao, Zuju Ma, Rongjian Sa, Zhitao Cui, Shuaishuai Gao, Wei Du, Xueqin Sun, and Qiaohong Li, Adsorption Behavior of Environmental Gas Molecules on Pristine and Defective MoSi₂N₄: Possible Application as Highly Sensitive and Reusable Gas Sensors. *ACS Omega* 7, 8706-8716 (2022).
 47. Kresse, G. & Furthmüller, J. Efficiency of ab-initio total energy calculations for metals and semiconductors using a plane-wave basis set. *Comput. Mater. Sci.* 6, 15–50 (1996).
 48. Kresse, G. & Furthmüller, J. Efficient iterative schemes for ab initio totalenergy calculations using a plane-wave basis set. *Phys. Rev. B* 54, 11169-11186 (1996).

49. Perdew, J. P., Burke, K. & Ernzerhof, M. Generalized gradient approximation made simple. *Phys. Rev. Lett.* 77, 3865-3868 (1996).
50. Perdew, J. P., Ernzerhof, M., Burke, K., Rationale for mixing exact exchange with density functional approximations. *J. Chem. Phys.* 105, 9982-9985 (1996).
51. J. Wellendorff, K. T. Lundgaard, A. Møgelhøj, V. Petzold, D. D. Landis, J. K. Nørskov, T. Bligaard & K.W. Jacobsen, Density functionals for surface science: Exchange-correlation model development with Bayesian error estimation. *Phys. Rev. B* 85, 235149 (2012).
52. Neugebauer, J. & Scheffler, M. Adsorbate-substrate and adsorbate-adsorbate interactions of Na and K adlayers on Al (111). *Phys. Rev. B* 46, 16067-16080 (1992).
53. Nørskov, J. K. et al. Origin of the overpotential for oxygen reduction at a fuelcell cathode. *J. Phys. Chem. B* 108, 17886-17892 (2004).
54. Mao, X. et al. Silicon-doped graphene edges: an efficient metal-free catalyst for the reduction of CO₂ into methanol and ethanol. *Catal. Sci. Technol.* 9, 6800-6807 (2019).
55. Frese Jr K. In *Electrochemical and Electrocatalytic Reactions of Carbon Dioxide* (eds. Sullivan, B.P., Krist, K., & Guard, H.E.). (Elsevier: New York, 1993).
56. Li, Y., Zhou, Z., Yu, G., Chen, W. & Chen, Z. C. O. Catalytic oxidation on iron-embedded graphene: computational quest for low-cost nanocatalysts. *J. Phys. Chem. C* 114, 6250–6254 (2010).
57. Li, F., Li, Y., Zeng, X. C. & Chen, Z. Exploration of high-performance single atom catalysts on support M₁/FeO_x for CO oxidation via computational study. *ACS Catal.* 5, 544–552 (2014).
58. Li, Y., Su, H., Chan, S. H. & Sun, Q. CO₂ electroreduction performance of transition metal dimers supported on graphene: a theoretical study. *ACS Catal.* 5, 6658–6664 (2015).
59. Back, S., Lim, J., Kim, N. Y., Kim, Y. H. & Jung, Y. Single-atom catalysts for CO₂ electroreduction with significant activity and selectivity improvements. *Chem. Sci.* 8, 1090–1096 (2017).
60. Bronsted, J. N. Acid and basic catalysis. *Chem. Rev.* 5, 231–338 (1928).
61. Evans, M. & Polanyi, M. Inertia and driving force of chemical reactions. *Trans. Faraday Soc.* 34, 11–24 (1938).